PAPER

Electron collision cross sections and electronic states of BH: an *R*-matrix study for fusion edge plasmas

IOP Publishing Plasma Physics and Controlled Fusion
Plasma Phys. Control. Fusion **67** (2025) 025009 (10pp) https://doi.org/10.1088/1361-6587/ada1fd

Electron collision cross sections and electronic states of BH: an *R*-matrix study for fusion edge plasmas

K Chakrabarti[1,*], N Mukherjee[1], A Bhattacharyya[2] and J Tennyson[3]

[1] Department of Mathematics, Scottish Church College, 1 & 3 Urquhart Sq., Kolkata 700 006, India
[2] Department of Physics, University of Calcutta, 92 A. P .C. Road., Kolkata 700 009, India
[3] Department of Physics and Astronomy, University College London, Gower Street, London WC1E 6BT, United Kingdom

E-mail: kkch.atmol@gmail.com

Received 21 September 2024, revised 11 December 2024
Accepted for publication 20 December 2024
Published 6 January 2025

Abstract

A detailed collision calculation of electron impact on BH at the BH equilibrium $R_e = 2.3285\,a_0$ is presented. First a good quality wave function for the target BH molecule is developed at the configuration interaction level. Then the *R*-matrix method is used to obtain collision cross sections for elastic scattering and state-to-state excitation to several excited electronic states of BH. The differential cross sections for elastic scattering below 10 eV and momentum transfer cross section are also obtained. Our calculations further yield two BH^- anionic bound states and a few e-BH anionic resonances which have not been previously reported. We obtain potential energy curves (PECs) for the two BH^- bound states of $^2\Pi$ and $^4\Sigma^-$ symmetries, and the PEC for the resonant BH^- state of $^2\Pi$ symmetry. These data will aid studies of edge plasma characteristics in tokamaks where boronization is used for wall conditioning.

Keywords: *R*-matrix method, cross section, boron hydride, fusion, edge plasma, boronization

1. Introduction

In fusion devices using magnetic confinement, wall conditioning of the plasma facing components (PFCs) is very important. Improper wall conditioning can lead to impurities in the plasma by erosion of wall material and hydrogenic recycling which can affect the overall core plasma performance. Wall conditioning methods such as boronization, siliconization, lithium pellet injection have been shown to significantly improve plasma wall interaction and core plasma performance [1, 2] and have been tested extensively in experimental tokamaks such as EAST, KSTAR and ASDEX Upgrade [3–6]. The International thermonuclear experimental reactor ITER (from Latin 'The Way') will also shift form using beryllium as the PFC in the main chamber to a full tungsten machine with boronized walls [7]. The immediate implication of this is the presence of boron and tungsten impurities in the plasma of which significant amounts may be that of boron and tungsten hydrides and their isotopologues. These can affect the plasma flow and can cause undesired deposition in the machine affecting performance. Detailed data in the form of cross sections and rates are therefore needed on the impurities for plasma flow modeling and understanding deposition.

Darby-Lewis and co-workers performed a series of electron collision and spectroscopic calculations on BeH (BeD and BeT) [8–10] to support analysis of plasma reactions with beryllium walls, particularly JET. These data formed the basis of a recent analysis of beryllium hydride isotopologue spectra produced by plasma-surface interactions during limiter and divertor JET-ILW (ITER-like Wall) pulses [11], which showed that hydride production was an important part of the wall erosion via chemical-assisted physical sputtering; the dependence on plasma and wall conditions was also monitored. It is therefore interesting to consider how the electron collision of properties BeH and BH differ. The goal of the present work

* Author to whom any correspondence should be addressed.

is to provide a detailed study of electron impact on BH, which can be a major impurity candidate, and also to provide molecular states of BH and its negative ion BH^-.

There are several studies on the BH and BH^- states of which we report only those performed after 1990, works prior to these can be seen from the references in the respective articles. Gagliardi *et al* [12] reported a full configuration interaction calculation of 20 low lying states of BH and obtained their potential energy curves (PECs), many of which were unreported before. They also obtained spectroscopic parameters for a few of the low lying states. Spectroscopic properties of 8 Λ-S and 23 Ω states of BH were recently reported by Wei *et al* [13]. A much more comprehensive calculation of the lowest 32 states of BH and two bound states of BH^- (together with three states of HBBH) was reported by Miliordos and Mavridis [14]. They not only gave the PECs of these states but also reported a very detailed study of binding energies, spectroscopic parameters and dipole moments among other parameters. This study is by far the most comprehensive work on BH and BH^- states available. A non Born–Oppenheimer calculation of the ground state BH was reported by Bubin *et al* [15], however, the focus here was more on the accuracy of the ground state and its dissociation energy rather than a comprehensive study of the other states.

Collisional studies on BH are largely absent except for the recent work by Kawate *et al* [16] where the authors used the QEC software package [17] to perform *R*-matrix calculations of cross sections for elastic scattering, electronic excitations from the ground state to the first six excited states of BH, and electron impact ionization of BH using the binary encounter Bethe (BEB) method [18].

In this work we present a more comprehensive study of cross sections for electron impact on BH and the molecular states of BH and BH^-; the target wave functions are represented using Slater basis functions, which generally give better results than Gaussian basis sets for compact representations such as those required for scattering calculations. We compute cross sections for elastic scattering, electron impact excitation to several electronically excited states of BH, differential cross sections (DCSs) for elastic scattering, momentum transfer cross sections (MTCSs) and have given an estimate of the electron impact dissociation cross section. Moreover, we also report anionic bound states of BH^- and one new anionic resonance of $^2\Pi$ symmetry.

2. The *R*-matrix method

Since we routinely use the *R*-matrix method for studying molecular states and electron collision problems, we only give a very brief description in the present work and point to some of our most recent works [19, 20] and to the review by Tennyson [21] for details. Our calculations used the linear molecule *R*-matrix code [22, 23] which uses Slater type orbitals (STOs) to represent the target wavefunction and numerical orbitals to represent the continuum.

In order to separate the short-range and long-range interactions so that they can be suitably treated by different methods, the configuration space is divided into an inner region, a sphere of radius a centered on the molecular center-of-mass of the N-electron target molecule, hopefully containing all short-range interactions, and an outer region exterior to it with other long-range interactions such as Coulomb interactions. An inner region $N+1$ electron wave function of the scattered electron and the N-electron target is then built using the following prescription,

$$\Psi_k^{N+1} = \mathcal{A}\sum_{i,j} a_{ijk}\Phi_i(1,\ldots,N)\,F_{ij}(N+1) + \sum_i b_{ik}\,\chi_i(1,\ldots,N+1), \quad (1)$$

where $\mathcal{A}$ is an antisymmetrisation operator, the N-electron target is represented by Φ_i, and in our calculations, F_{ij} are numerical continuum orbitals based on Bessel functions. The square integrable functions $\chi_i(1,\ldots,N+1)$ are called L^2 functions and are constructed to include electron correlation and polarization of the target in the field of the incident electron. The parameters a_{ijk} and b_{ik} are variationally determined.

Once Ψ_k^{N+1} is determined, it is used to construct an energy-dependent R-matrix $\mathbf{R}(r,E)$ at the boundary of the inner and outer regions which is related to the logarithmic derivative of the radial part $\mathbf{f}(r)$ of Ψ_k^{N+1} by

$$\mathbf{R}(r,E) = \mathbf{f}(r)\left[r\,\mathbf{f}'(r)\right]^{-1}, \quad (2)$$

where r is the radial coordinate and a Buttle correction [24] is needed on the boundary to relax the boundary conditions used to compute the inner region numerical continuum functions. The R-matrix is then propagated in the outer region to a suitable asymptotic distance $R_{\rm asy}$ and matched with known asymptotic functions obtained from a Gailitis expansion [25]. This matching yields the K-matrix from which the T-matrix is derived. Finally all scattering observables are extracted from the T-matrix. The detection of resonances and bound states however, do not require the T-matrix and are discussed in subsequent sections.

3. Target calculations

The diatomic version of the UK molecular *R*-matrix codes [22, 23], which uses Slater functions to represent the target and scattering states, are used for the present study. We used the STO basis set of Cade and Huo [26] centered on the B atom containing 5 s-type, 4 p-type, 2 d-type and 1 f-type type basis functions. For the STOs centered on the H atom, we used the basis set II of Langhoff *et al* [27] after removing 3 p-type functions to avoid linear dependence. The resulting *trimmed* basis set containing 4 s-type and 1 p-type functions centered on the H atom was used for all subsequent calculations.

A set of 29 molecular orbitals (MOs) consisting of 17 σ, 8 π, 3 δ and 1 ϕ orbitals was first built from the STOs and

Table 1. Comparison of vertical excitation energies (VEE) and adiabatic excitation energies (T_e) (in eV) from the X $^1\Sigma^+$ ground state of the BH molecule, and the equilibrium bond length R_e (in a_0). The following target models, namely M1, M2 and M3 have been used for the comparison. M1: $(1\sigma)^2(2-8\sigma,1-2\pi)^4$, M2: $(1\sigma)^2(2-8\sigma,1-3\pi)^4$, M3: $(1\sigma)^2(2-10\sigma,1-3\pi)^4$. Reprinted from [14], with the permission of AIP Publishing.

Target states	VEE M1	VEE M2	VEE M3	T_e M3	T_e M&M[a]	VEE[b] reference [16]	R_e M3	R_e Exp[d]
X $^1\Sigma^+$	0.00	0.00	0.00	0.00	0.00	0.00	2.3285	2.3285
1 $^3\Pi$	1.53	1.27	1.33	1.31	0.98	1.33	2.35	2.27
1 $^1\Pi$	3.29	3.16	3.11	2.87	2.78	3.12	2.35	2.30
1 $^3\Sigma^-$	5.43	4.62	4.65	4.68	4.35	4.66	2.35	2.32
1 $^1\Delta$	6.85	6.26	6.38	5.84	6.25	6.40	2.35	2.26
2 $^3\Pi$	8.60	8.15	8.01	6.27	—	5.88	3.82	3.66[c]
1 $^3\Sigma^+$	6.35	6.30	6.30	6.41	—	—	—	—
2 $^1\Sigma^+$	6.58	6.54	6.52	6.52	7.32	6.54	2.35	2.30
3 $^1\Sigma+$	7.64	7.14	7.22	6.96	—	7.24	2.35	2.29[c]
2 $^3\Sigma^+$	8.85	8.88	8.67	7.34	10.71	8.11	2.84	2.30[c]

[a] Miliordos and Mavridis [14].
[b] Kawate *et al* [16].
[c] MRCI value quoted from [14] since an experimental value is not available.
[d] Experimental values quoted from table III of [14]

were used to make an initial SCF calculation on the BH X $^1\Sigma^+$ ground state and the 1 $^3\Pi$ excited state. Finally 17 σ, 8 π and 3 δ SCF orbitals were used in large complete active space (CAS) configuration interaction (CI) calculations on the BH target. These calculations froze the B 1*s* orbitals (the 1σ orbital) giving 4 active electrons. Tests showed that calculations with the MOs constructed from the 1 $^3\Pi$ SCF orbitals gave much better results for the vertical excitation energies (VEEs) of the target BH molecule than MOs constructed from the X $^1\Sigma^+$ SCF orbitals. All subsequent calculations reported here therefore used MOs constructed from the 1 $^3\Pi$ SCF orbitals.

We tested many target models out of which we present three of the most significant in table 1. Clearly the VEEs obtained with our CI model M3, with the exception of the VEEs of the 2 $^3\Pi$ and 2 $^3\Sigma^+$ states for which deviations are slightly larger, are in excellent agreement with the adiabatic excitation energies T_e of Miliordos and Mavridis [14] (henceforth M&M) which were obtained using a much more sophisticated multi-reference CI (MRCI) calculation. The higher values of the VEEs of the 2 $^3\Pi$ and 2 $^3\Sigma^+$ from our calculation is likely because M&M give adiabatic values T_e, whereas we give the VEEs and these can be significantly different if the minima of the PECs do not coincide. On the other hand, the VEEs of Kawate *et al* [16], shown in the last column of table 1 and computed with a significantly smaller CI model and Gaussian basis sets, deviate significantly for the higher excited states from those of M&M. We therefore performed subsequent calculations with our target model M3 defined by $(1\sigma)^2(2-10\sigma,1-3\pi)^4$, where 2 electrons were frozen in the 1σ orbital and the remaining 4 electrons were movable in the CAS defined by $(2\sigma-10\sigma,1\pi-3\pi)$.

Figure 1 shows the PECs of the first 10 BH target states used in the present work where we have relabeled the states to make their identification easier and have not followed the labeling scheme of M&M which are sometimes arbitrary. The curves are very similar to the ones obtained by M&M, except for the

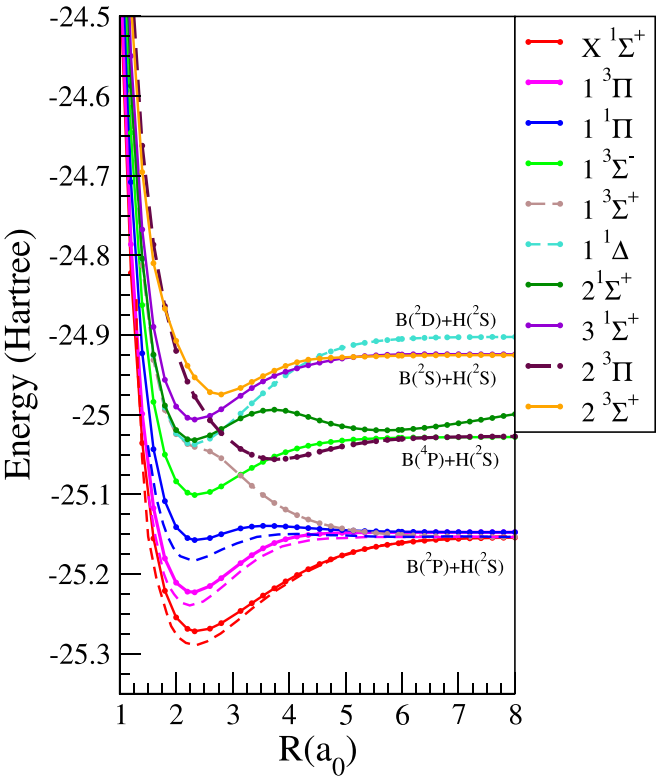

Figure 1. First 10 potential energy curves of the BH target states used in the present calculation. The dashed curves are the corresponding states of M&M. All curves from the present calculation have been shifted down uniformly by 0.0714 Hartree to make the asymptotic limits of the present curves approaching B(^2P)+H(^2S) the same as that of M&M. Reprinted from [14], with the permission of AIP Publishing.

1 $^1\Delta$ (C $^1\Delta$ in M&M) curve which we find to be slightly above the 1 $^3\Sigma^+$ state, while M&M find that this curve goes slightly below the 1 $^3\Sigma^+$ state. However, this difference is small, since

the difference between the minima of the $1\,^1\Delta$ state in the two cases is only about 0.54 eV, as can be seen from table 1. For comparison, we also include the first three states, namely the $X\,^1\Sigma^+$ state, $1\,^3\Pi$ and the $1\,^1\Pi$ states of M&M in figure 1.

The value of the dipole moment μ for the $X\,^1\Sigma^+$ ground state at the BH equilibrium ranges between 1.3 D and 1.73 D in available literature (see [14]). The magnitude of the dipole moment $\mu(X\,^1\Sigma^+)$ at the BH equilibrium was found by us to be 1.36 D, which is in excellent agreement with the corresponding values in literature.

4. Scattering models

For the scattering calculations, 13 BH SCF orbitals and a CAS given by model M3 above were used. The target SCF orbitals were supplemented by numerical continuum orbitals F_{ij} describing the scattered electron, and were obtained as partial wave expansion around the centre-of-mass. Partial waves with $l \leqslant 6$ and $m \leqslant 2$ were retained in the calculation as these proved sufficient to converge the cross sections. Since the target was neutral, the radial parts of the continuum functions F_{ij} were chosen to be solutions of the spherical Bessel equation and those solutions with energy less than 6 Ryd were retained in the calculation. An R-matrix radius of $11\,a_0$ was used giving 127 (51σ, 42π and 34δ continuum functions) which were Schmidt orthogonalised to the target SCF orbitals [28]. Finally this resulting set of orthogonalized orbitals were used in all scattering calculations reported here, and were performed at the target equilibrium $R_e = 2.3285\,a_0$.

We extensively tested scattering models and our final calculations used a 10-state model as described in table 2, where the number and symmetry of the target states coupled for each e+BH overall symmetry are detailed. We also performed calculations in 8 and 12-state (changes shown in table 2) models, obtained by deleting or adding two states in the 10-state model, to check convergence in cross sections. However, we do not give the details of these to maintain conciseness.

5. Results

5.1. Cross sections

For the calculation of cross sections, the R-matrix was propagated to $120\,a_0$ and then matched with asymptotic functions to obtain the K-matrix which was then used to get the T-matrix given by

$$\mathbf{T} = 2\iota\mathbf{K}\left(1 - \iota\mathbf{K}\right)^{-1}, \tag{3}$$

where $\iota = \sqrt{-1}$. Finally, all cross sections were obtained form the T-matrix.

5.1.1. Elastic scattering. We calculated cross sections using the 8, 10 and 12-state scattering models described above. Since the target ground state is of $^1\Sigma^+$ symmetry, for scattering from the ground state, the states with quartet overall e+BH spin multiplicity do not contribute to the cross section. Similarly the Σ^+ symmetry of the ground state forbids contribution from the Σ^- e+BH overall symmetry.

The left panel of figure 2 shows the elastic cross sections in the 8, 10 and 12-state scattering models. Convergence is clearly obtained with the 10 and 12-state models. However, the 12-state model shows several spurious resonances, for example near 2 eV. From past experience [29], these spurious resonances are caused by diffuse target states which leak outside the R-matrix inner region. We therefore chose to present all cross sections in the 10-state model. The elastic cross section shows a broad shape resonance like structure around 1 eV. In the right panel of figure 2 we have tried to trace the origin of this broad resonance and have shown that this broad resonance arises from the $^2\Sigma^+$ component of the cross section. Further, we calculated the $^2\Sigma^+$ component of the elastic cross section in the static exchange (SE) model and the results are shown in the bottom panel of figure 2. Since the broad resonance appears both in the SE and the close coupling (CC) calculations, this is likely to be a shape resonance. In the SE calculation this resonance is detected at an energy 0.0742 Ryd $\approx$ 1.01 eV with a width 0.258 Ryd $\approx$ 3.51 eV, and is likely to be associated with a higher l partial wave, since s-wave scattering cannot give rise to shape resonances (see for example [21]).

The polar nature of the molecule cases a sharp peak in the cross section at low energies due to the long range potential associated with the dipole moment. This means that we need to include partial waves greater than $l = 6$. The effect of these missing partial waves may be taken into account using Born approximation by adjusting the total cross sections [30]. We therefore included the Born correction to the elastic cross section, which is shown on the right panel of figure 2. We also show the Born corrected cross sections of Kawate *et al* [16], which agrees very well with the present Born corrected cross elastic sections both in magnitude and shape.

A comprehensive set of cross sections, including the elastic cross section, was also given recently by Kawate *et al* [16] (abbreviated henceforth to KMG). They used the R-matrix method with Gaussian basis sets, in contrast to ours where we used Slater bases. The shape of the elastic cross section curve given by KMG is somewhat different from ours at the low energy end and misses the broad $^2\Sigma^+$ resonance near 1 eV and the narrow $^2\Pi$ resonance observed in our elastic cross section curve. In our perception, the reason for this could be the following. KMG used a minimum of 16 target states in the CC expansion in equation (1) to calculate the inner region wave function Ψ_k^{N+1} from which they derived the cross sections. However, from table 1 above, it is clear that beyond the first few target states, their VEEs progressively become too high. For example, for the $2\,^3\Sigma^+$ state their VEE is approximately 2 eV above the corresponding VEE given by our model M3. For higher target states, the VEEs are not documented by KMG, but the deviations are likely to be even greater as appears from the trend in table 1. This is an indication that their corresponding target state wave functions become increasingly inaccurate for the higher excited states, which ultimately

Table 2. Symmetry and number of states used in the close coupling equation (1) in the 10-state model. The changes in the number of states included in the 12-state model is indicated in brackets.

Symmetry	Number	Target states coupled
$^2\Sigma^+$	10 (12)	Three $^1\Sigma^+$, one (two) $^1\Pi$, one $^1\Delta$, two (three) $^3\Sigma^+$ three $^3\Pi$
$^2\Pi$	10 (12)	Three $^1\Sigma^+$, one (two) $^1\Pi$, one $^1\Delta$, two $^3\Sigma^+$, one $^3\Sigma^-$ and two (three) $^3\Pi$
$^2\Sigma^-$	10 (12)	Three (four) $^1\Pi$, one $^1\Delta$, one (two) $^3\Sigma^-$, four $^3\Pi$ and one $^3\Delta$
$^2\Delta$	10 (12)	Three $^1\Sigma^+$, one (two) $^1\Pi$, one $^1\Delta$, two $^3\Sigma^+$, one $^3\Sigma^-$ and two (three) $^3\Pi$
$^4\Sigma^+$	10 (12)	Four $^3\Sigma^+$, four $^3\Pi$ and two (four) $^3\Delta$
$^4\Pi$	10 (12)	Three (four) $^3\Sigma^+$, two (three) $^3\Sigma^-$, four $^3\Pi$ and one $^3\Delta$
$^4\Sigma^-$	10 (12)	Three (four) $^3\Sigma^-$, four $^3\Pi$ and three (four) $^3\Delta$
$^4\Delta$	10 (12)	Three (four) $^3\Sigma^+$, two (three) $^3\Sigma^-$, four $^3\Pi$ and one $^3\Delta$

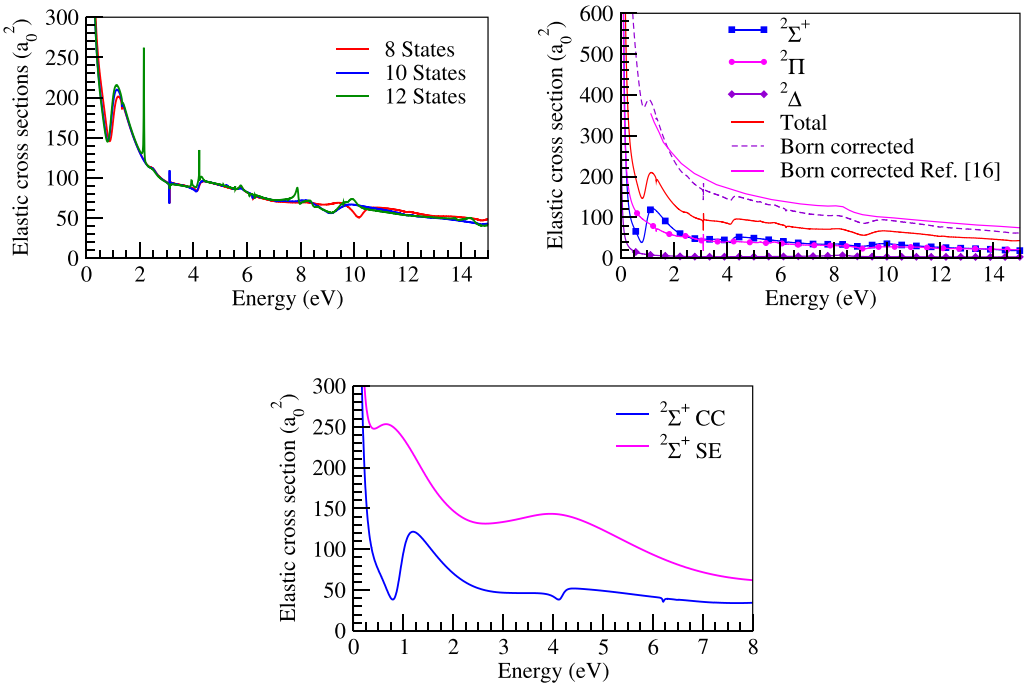

Figure 2. Top left panel: elastic cross section for electron scattering from BH calculated in the 8, 10 and 12 state models discussed in the text. Top right panel: contribution to the elastic cross section from each of the e+BH overall symmetries as indicated in the legend. The top most dashed curve is the Born corrected elastic cross section. Shown also is the Born corrected cross section of Kawate *et al*. Bottom panel: $^2\Sigma^+$ component elastic cross section in the static exchange (SE) and the close coupling (CC) calculations. The broad resonance feature around 1 eV in both curves confirms this to be due to a shape resonance. Reproduced from [16].

leads to lower quality inner region wave function when large number of target states are coupled. This may cause significant effects on the cross sections. For example, the elastic cross section estimated from figure 1 of KMG at 2 eV is approximately $66\,a_0^2$ which is nearly half that of the present calculation $131\,a_0^2$. In fact, as may be seen by comparing corresponding elastic cross section figures, much of the underlying physics is also ultimately lost due to inaccuracies of the inner region wave functions.

5.1.2. Electronic excitation. Figure 3 shows our cross sections for electronic excitation of the BH molecule form its X $^1\Sigma^+$ ground state to the first three singlet (left panels) and triplet (right panels) excited states. For the allowed transitions, we provide the Born corrected cross sections which are shown as the dashed curve in the respective figures. The Born corrected cross sections are approximately double the magnitude of the uncorrected cross sections at the high energy end.

Cross sections for the same electronic excitations have also been reported by Kawate *et al* [16] (KMG). As with the elastic cross sections discussed above, the excitation cross section curves of KMG do not fully agree with ours and misses out many structures shown by our cross section curves. We also point out two major issues with the cross sections given by KMG. Firstly, their Born corrected cross section for the 2 $^1\Sigma^+$

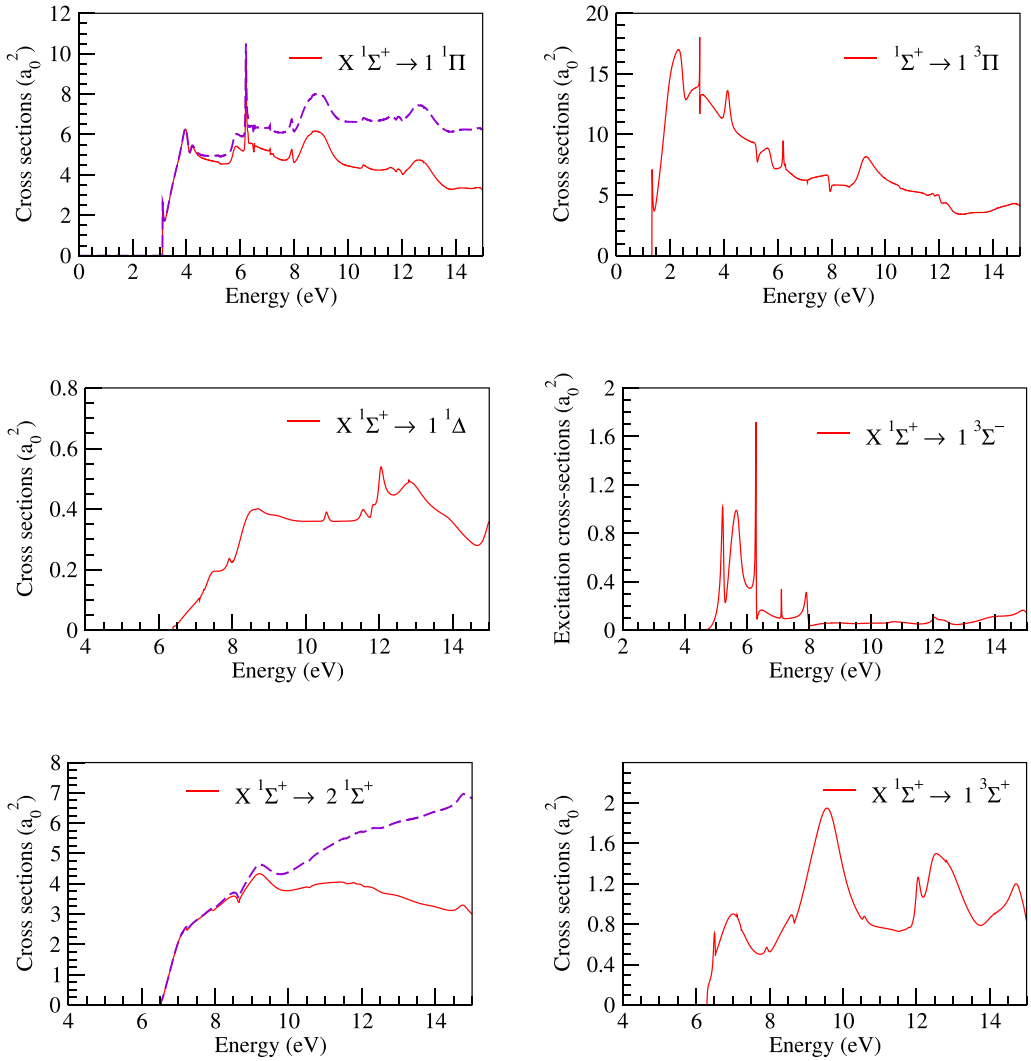

Figure 3. Cross sections for electronic excitation of BH form its X $^1\Sigma^+$ ground state to the first three singlet (left panels) and triplet (right panels) excited states. The Born corrected cross sections corresponding to the allowed transitions are shown as dashed curves.

state (labelled as B $^1\Sigma^+$ state in their work [16]) do not agree with ours for energies greater than 10 eV. The likely cause of this may be a lower value of the transition dipole moment (TDM) used for the calculation of the Born correction. While we find a TDM of magnitude 1.88 a.u. for X $^1\Sigma^+ \rightarrow 2\ ^1\Sigma^+$ transition, the value of the TDM quoted, and likely used, in the calculations by KMG is 0.35 a.u. (converted from 0.8937 D given in table 1 for the cc-pVTZ basis set calculation) which is lower than ours. Secondly, the threshold for the X $^1\Sigma^+ \rightarrow 1\ ^3\Sigma^+$ used by KMG (labeled c $^3\Sigma^+$ in their work) appears to be too high. Moreover, the shape of their cross section curve for this excitation is very different form ours. From these considerations, it seems likely that KMG have taken the 2 $^3\Sigma^+$ as their c $^3\Sigma^+$ state, while the 1 $^3\Sigma^+$ was completely missed. Accordingly, we therefore identify the c $^3\Sigma^+$ state of KMG with the 2 $^3\Sigma^+$ state in table 1, rather than the 1 $^3\Sigma^+$ state.

5.1.3. Differential and MTCSs. Neglecting the projectile spin state and the target rotational state, the DCS for state-to-state transition from the target state i to a state j is given by [31]

$$\left(\frac{\mathrm{d}\sigma}{\mathrm{d}\Omega}\right)_{ij} = \sum_k A_{ij}^k P_k(\cos\vartheta), \tag{4}$$

where P_k are Legendre polynomials, the coefficients A_{ij}^k are found using the T-matrix, the details of which may be obtained from [31]. An adapted version of the DCS code of Malegat [31], that requires T-matrices from R-matrix calculation as input, was used to calculate the elastic DCS below 10 eV.

The left panel of figure 4 shows our elastic DCS for four values of the incident energies below 10 eV. All the DCS curves show deep minima around 100°. Overall the magnitude of the DCS decrease with increase of incident energy and are large in the forward and backward directions.

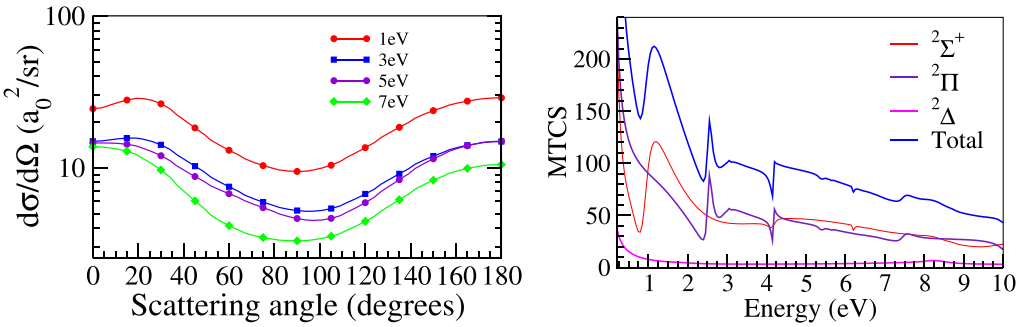

Figure 4. Left panel: elastic differential cross section for electron scattering from BH. Right panel: momentum transfer cross section (MTCS). Shown also are the contribution to the MTCS for each symmetry.

Figure 4 right panel shows our MTCS which can be calculated from the the DCS using the relation

$$\sigma_{\rm MTCS} = \int (1-\cos\theta)\,\frac{{\rm d}\sigma}{{\rm d}\Omega}\,{\rm d}\Omega. \qquad (5)$$

The MTCS cross section shows many features of the total elastic cross section. Particularly, the broad peak near 1.5 eV arising from the $^2\Sigma^+$ component and the sharp $^2\Pi$ resonance near 2.5 eV is also visible in the total elastic cross section.

Leider *et al* [32] discuss the decay rate per photon for the main spectroscopic band the dipole allowed A $^1\Pi \rightarrow$ X $^1\Sigma^+$ band. The excitation rate is obtained by integration over a Maxwellian distribution for electrons with which KMG [16] calculate the decay rate per photon using the ratio of the ionization plus dissociation rate to the excitation rate; this calculation also involved extrapolating cross sections beyond 10 eV. We discuss our estimated dissociation cross section below but have not calculated the ionization rate. It would appear, however, that our rate will be about 30% of that predicted by KMG.

5.1.4. Estimate of electron impact dissociation. The first dissociation threshold of BH is about 3.53 eV and correlates to the limit B(^2P)+H(^2S). The states approaching this dissociation limit are the X $^1\Sigma^+$, 1 $^3\Pi$, 1 $^1\Pi$ and the 1 $^1\Sigma^-$ states. To calculate the dissociation cross section, we assumed that excitations to the states correlating to the B(^2P)+H(^2S) limit above the dissociation threshold leads to dissociation through the B(^2P)+H(^2S) channel. Thus for each incident energy above the dissociation threshold, we calculated excitation cross sections for the states approaching this threshold and finally summed over the cross sections to get the dissociation cross section for that energy. This method, although approximate, has always yielded fair estimates of the dissociation cross section in earlier cases (see for example [33]).

Figure 5 shows the dissociation cross section through the dissociation channel B(^2P)+H(^2S). The cross section are obtained using the Born corrected excitation cross sections wherever applicable. Overall the cross sections decrease with increasing incident energy due to opening of other competing

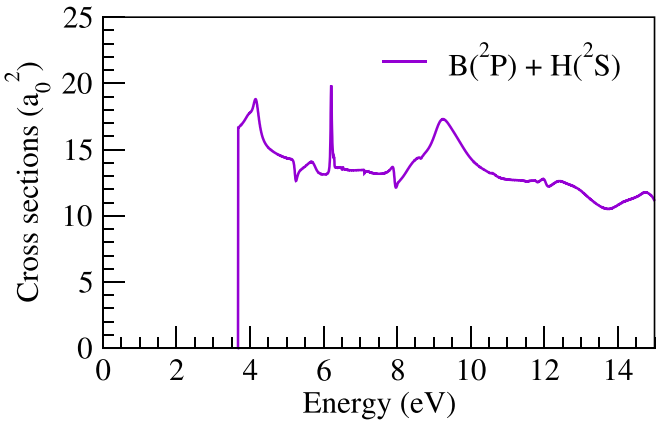

Figure 5. Cross section for electron impact dissociation of the BH molecule through the B(^2P)+H(^2S) dissociation channel.

excitation and dissociation channels. However, as no experimental data is as yet available we are not in a position to compare or give any accuracy of our data.

5.2. Bound states and resonances

5.2.1. Bound states. The $N+1$ electron inner region can represent a bound state in R-matrix calculations provided it is made to satisfy appropriate boundary conditions for large values of the radial coordinate. In the present case, the R-matrix was propagated to an asymptotic distance $R_{\rm asy}$ and matched with exponentially decaying functions. Generally $R_{\rm asy} = 40\,a_0$ proved sufficient for bound state calculations, however for the $^2\Pi$ bound state calculation, a lower value of $R_{\rm asy}$ was sometimes needed. Also the R-matrix radius needed to be progressively increased from $10\,a_0$ at $R = 1$ to $15\,a_0$ for $R = 7\,a_0$ to prevent the inner region wave function from leaking out of the R-matrix box. After the matching at $R_{\rm asy}$, the bound states can be shown to be the roots of an energy dependent determinant $\mathcal{B}(E)$, and were found by searching over a suitable energy grid. The method is extensively discussed by Sarpal *et al* [34] and is not detailed here to avoid repetition.

Our calculations found two bound states of $^2\Pi$ and $^4\Sigma^-$ symmetry both of which were reported by M&M [14] and

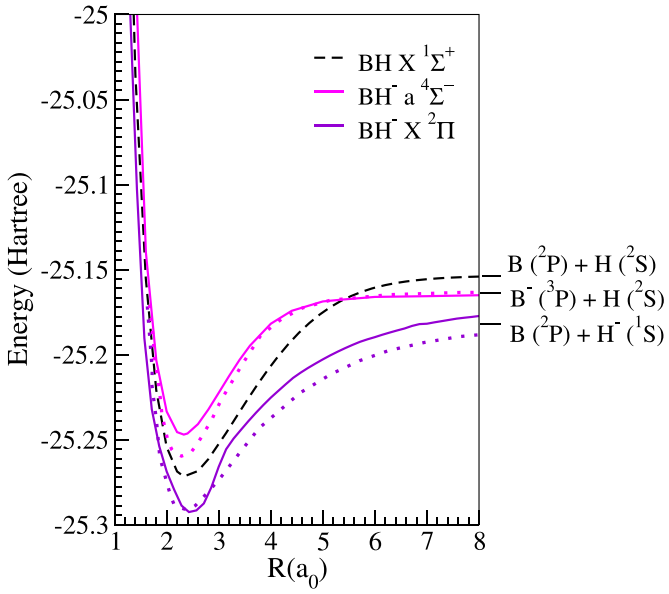

Figure 6. Bound state PECs of BH and BH$^-$. Dashed curve: BH X $^1\Sigma^+$ ground state from present calculation. Continuous curves: top—BH$^-$ a $^4\Sigma^-$ bound state and bottom—BH$^-$ X $^2\Pi$ ground state from present calculation. Dotted curves: bottom—X $^2\Pi$ and top—a $^4\Sigma^-$ state of M&M. All curves from the present calculation have been shifted down uniformly by 0.0714 Hartree. Reprinted from [14], with the permission of AIP Publishing.

are shown in figure 6 after shifting all R-matrix curves down uniformly by 0.0714 Hartree so that the asymptotic limit of the BH$^-$ a $^4\Sigma^-$ curve coincides with that of M&M. We also show the corresponding curves of M&M [14] (dotted curves in figure 6) which agree reasonably well in shape and well depth with the curves from our present calculation.

5.2.2. Resonances. It is well known that anionic resonances play a very important role in dissociative electron attachment (DEA) to neutral molecules. We therefore made efforts to find anionic resonances in the e+BH system. For resonance detection, the R-matrix was propagated to $R_{\rm asy} = 120\,a_0$ and matched with asymptotic functions to obtain the K-matrix. Resonances were detected and fitted to a Breit-Wigner profile to obtain their energy position E and their width Γ using the RESON program of Tennyson and Noble [35] using an energy grid 0.005 eV.

Table 3 shows some of the low lying resonances we detected at the BH equilibrium $R_{\rm e} = 2.3285\,a_0$. The $^2\Pi$ resonance has a narrow width and is a Feshbach resonance with 1 $^3\Pi$ state as its parent state since it lies above the X $^1\Sigma^+$ and below 1 $^3\Pi$ states. The first $^2\Sigma^+$ resonance appears in the SE calculation around 1 eV and has a large width of about 0.26 Ryd $\approx$ 3.54 eV, due to which we think that that this should be a shape resonance. The signature of this resonance can be found in the $^2\Sigma^+$ component of the CC and SE elastic cross sections (figure 2) as a broad peak near 1 eV. The next $^2\Sigma^+$ resonance appears above the 1 $^1\Pi$ target state and is also a Feshbach resonance. The states immediately above the 1 $^1\Pi$ target state are

Table 3. Resonance positions and widths (in Rydbergs) of some of the low lying resonances in the e-BH system at $R_{\rm e} = 2.3285\ a_0$.

State	Position	Width
Above X $^1\Sigma^+$ state		
$^2\Pi$	0.003 98	0.001 15
$^2\Sigma^+$	0.074 23	0.2581[a]
Above 1 $^1\Pi$ state		
$^2\Sigma^+$	0.3057	0.0161

[a] Likely a shape resonance detected by time delay method and SE calculation.

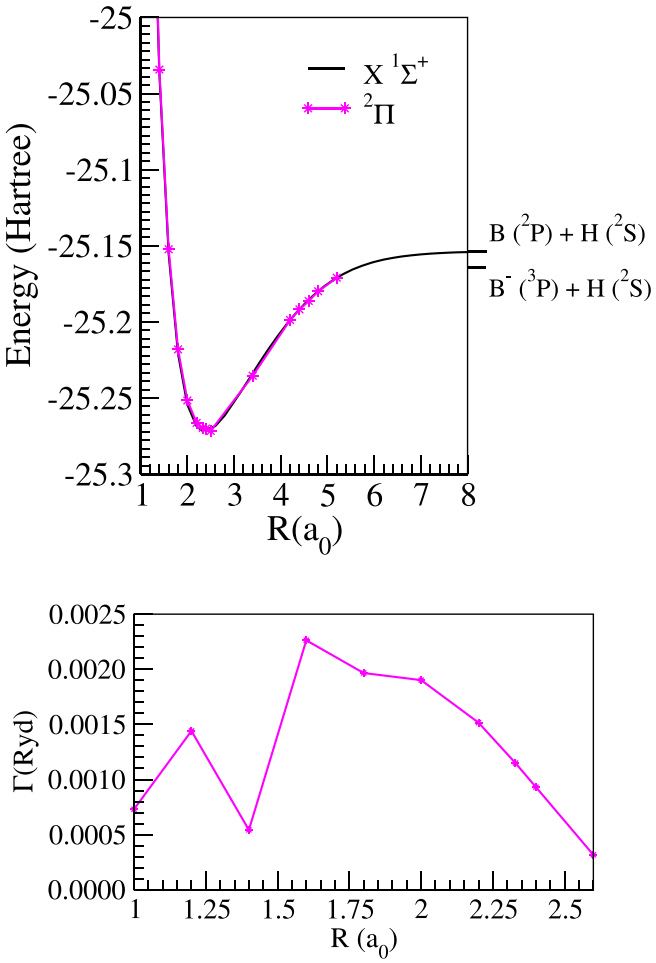

Figure 7. BH X $^1\Sigma^+$ ground state, BH$^-$ $^2\Pi$ resonant state and corresponding resonance width. Top panel: curve with symbols—BH$^-$ $^2\Pi$ resonant state. Bottom panel: resonance width for the $^2\Pi$ resonance.

the 1 $^3\Sigma^-$ and the 1 $^3\Sigma^+$ target state. From symmetry considerations, the incident electron cannot bind to the 1 $^3\Sigma^-$ state to give the $^2\Sigma^+$ resonance. We are therefore of the view that this resonance is likely to have the 1 $^3\Sigma^+$ state as its parent state.

The starred curve of the top panel in figure 7 shows the $^2\Pi$ resonance we have detected. The resonance becomes bound after $R = 2.5\,a_0$ and, since the resonance is of $^2\Pi$ symmetry, the resonance curve correlates with the B$^-$(^3P) + H(^2S)

asymptotic limit. We are able to detect a number of bound states below the BH X $^1\Sigma^+$ ground state which, in our perception, should correlate to this resonance. The process of correlating bound states with the resonance is harder for anionic resonances as they can not be categorised by their quantum defects as in the case of neutral resonances (see for example our work [36]). To construct the resonance curve in figure 7 we have also interpolated the bound state at $R = 3.4\,a_0$ to make our curve smooth as we could not detect any bound state between $R = 2.6$–$4.0\,a_0$.

From figure 7 it is clear that the $^2\Pi$ resonance lies very close to the BH ground state. Moreover, from the bottom panel of figure 7 we find that the width of this resonance is also very narrow, which means that this resonance is very stable and almost bound. We tried to estimate the DEA cross section using the approach of Munro *et al* [37], which uses model potentials and a survival factor for the resonance, using the $^2\Pi$ resonance and its width at the equilibrium $R_e = 2.3285\,a_0$. However, we found the DEA cross section estimates too be insignificantly small which is line with the fact that the resonance is so low energy that exciting it does not leave the system with enough energy to dissociate.

6. Conclusion

As discussed in the introduction, boronization of walls are being tested at many tokamak facilities and is also expected in the International thermonuclear experimental reactor ITER. With the aim of providing both molecular and cross section data on BH, which is expected to be present significantly in tokamaks with boronized walls, in this work we extensively study electron collision with BH. We provide the PECs of the BH target states. Using the *R*-matrix method we provide cross sections for elastic scattering, electronic excitation to the first six excited states of BH, and, using the excitation cross sections, we also provide an estimate of electron impact dissociation through the lowest B(^2P)+H(^2S) dissociation channel. We also provide elastic differential and momentum transfer crosssections. Probably the most important excitation cross section is X $^1\Sigma^+ \rightarrow$ A $^1\Pi$ (1 $^1\Pi$ in our notation) since emission has been observed from the A $^1\Pi$ state have been observed in plasma reactors [38]. We note that a detailed spectroscopic model, similar to that available for BeH/BeD/BeT [9], is under construction at UCL.

We further investigated the BH anionic bound and resonant states and are able to obtain two bound states, namely the X $^2\Pi$ ground state and the a $^4\Sigma^-$ excited state of BH^-. These states have been obtained before and our PECs agree reasonably with those of earlier calculations of Mliordos and Mavridis [14]. Our calculations yielded a single resonance of $^2\Pi$ symmetry which was unreported before. However, due to its very narrow width, this resonance appears fairly stable and is not likely to be an intermediate state for DEA. In fact, we found the DEA estimates via this resonance too small to be significant.

Comparing electron collisions with BH and BeH leads to some important differences. For BeH, the dominant electron impact excitation is the dipole allowed X $^2\Sigma^+ \rightarrow$ A $^2\Pi$ excitation with a threshold of about 2.5 eV, the cross section for which is nearly an order of magnitude larger than any of the other electronic excitations considered [8]. It is this state for which emission spectra are monitored [11]. For BH the corresponding excitation is the dipole allowed X $^1\Sigma^+ \rightarrow$ A $^1\Pi$ (1 $^1\Pi$ in our notation) with a threshold just below 3 eV; emissions from this state have been observed in plasma reactor studies [38]. However, we note that our calculations suggest that X $^1\Sigma^+ \rightarrow$ A $^1\Pi$ cross section, while larger than other singlet excitations, is only about half that predicted for the corresponding transition in BeH. Unlike BeH, BH has a lower-lying higher spin state and our calculations also consider electron-impact excitation of X $^1\Sigma^+ \rightarrow$ a $^3\Pi$ (1 $^3\Pi$ in this work) with a threshold of about 1.5 eV. While this excitation is not dipole allowed, our calculations still suggest that in the 3 eV region this excitation actually has a larger cross section than excitation of the A $^1\Pi$ state.

Data availability statement

The data that support the findings of this study will be openly available following an embargo at the following URL/DOI: https://amdis.iaea.org/db/collisiondb/. Data will be available from 2025 March 15.

Acknowledgments

KC acknowledges financial support from the International Atomic Energy Agency under the IAEA Coordinated Research Project F43027 'Formation and Properties of Molecules in Edge Plasmas' and IAEA Research Contract No. 28197. KC also acknowledges institutional financial support from Scottish Church College to the IAEA Research Contract No. 28197.

ORCID iDs

K Chakrabarti https://orcid.org/0000-0003-0013-5610
A Bhattacharyya https://orcid.org/0000-0002-2386-515X
J Tennyson https://orcid.org/0000-0002-4994-5238

References

[1] Peng L, Sun J, Sun Z, Gao F, Bonnin X and Liu J Y 2021 *Nucl. Mater. Energy* **26** 100937
[2] Winter J 1996 *Plasma Phys. Control. Fusion* **38** 1503
[3] Sun Z *et al* 2019 *Nucl. Mater. Energy* **19** 124
[4] Bortolon A *et al* 2019 *Nucl. Mater. Energy* **19** 384
[5] Sun Z *et al* 2021 *Nucl. Fusion* **61** 014002
[6] Sun L, Wu D, Li C, Wu J, Hong S, Bang E, Hu Z, Ding F, Luo G and Ding H 2022 *Nucl. Mater. Energy* **31** 101174
[7] (Available at: www.iter.org/whatsnew/print/396)
[8] Darby-Lewis D Z and Tennyson J 2017 *J. Phys. B: At. Mol. Opt. Phys.* **50** 175201

[9] Darby-Lewis D, Tennyson J, Lawson K D, Yurchenko S N, Stamp M F, Shaw A, Brezinsek S 2018 *J. Phys. B: At. Mol. Opt. Phys.* **51** 185701
[10] Darby-Lewis D, Tennyson J, Yurchenko S N and Lawson K D 2020 *J. Phys. B: At. Mol. Opt. Phys.* **53** 135202
[11] Pawelec E, Borodin D, Brezinsek S, Dittmar T, Douai D, Mazur D, Meigs A, Shaw A and Thomas B Contributors J and Exploitation E T 2024 *Phys. Plasmas* **31** 042516
[12] Gagliardi L, Luigi Bendazzoli G and Evangelisti S 1997 *Mol. Phys.* **91** 861–72
[13] Wei X, Sheng-Zhou L, Jin-Feng S, Wen-Tao L, Zun-Lüe Z and Feng L 2022 *Acta Phys. Sin.* **71** 103101
[14] Miliordos E and Mavridis A 2008 *J. Chem. Phys.* **128** 144308
[15] Bubin S, Stanke M and Adamowicz L 2009 *J. Chem. Phys.* **131** 044128
[16] Kawate T, Murakami I and Goto M 2023 *Plasma Sources Sci. Technol.* **32** 085006
[17] Cooper B *et al* 2019 *Atoms* **7** 97
[18] Kim Y and Rudd M E 1994 *Phys. Rev.* A **50** 3954–67
[19] Chakrabarti K and Dinda S 2023 *Plasma Phys. Control. Fusion* **65** 085017
[20] Chakrabarti K, Neogi P and Nandi G 2024 *Phys. Chem. Chem. Phys.* **26** 21659–67
[21] Tennyson J 2010 *Phys. Rep.* **491** 29–76
[22] Gillan C J, Tennyson J and Burke P G 1995 The UK molecular R-matrix scattering package: a computational perspective *Computational Methods for Electron-Molecule Collisions* ed W Huo and F A Gianturco (Plenum) pp 239–54
[23] Morgan L A, Tennyson J and Gillan C J 1998 *Comput. Phys. Commun.* **114** 120–8
[24] Buttle P J A 1967 *Phys. Rev.* **160** 719–29
[25] Noble C J and Nesbet R K 1984 *Comput. Phys. Commun.* **33** 399
[26] Cade P E and Huo W 1973 *At. Data Nucl. Data Tables* **13** 415
[27] Langhoff S R, van Dishoeck E F, Wetmore R and Dalgarno A 1982 *J. Chem. Phys.* **77** 1379
[28] Tennyson J, Burke P G and Berrington K A 1987 *Comp. Phys. Commun.* **47** 207–12
[29] Gorfinkiel J D, Morgan L A and Tennyson J 2002 *J. Phys. B: At. Mol. Opt. Phys.* **35** 543–55
[30] Kaur S, Baluja K L and Tennyson J 2008 *Phys. Rev.* A **77** 032718
[31] Malegat L 1990 *Comp. Phys. Commun.* **60** 391–404
[32] Lieder G, Behringer K and Field A R 1994 Spectroscopic investigation of molecular impurities in the ASDEX Upgrade divertor
[33] Ghosh R, Chakrabarti K and Choudhury B S 2022 *Plasma Sources Sci. Technol* **31** 065005
[34] Sarpal B K, Branchett S E, Tennyson J and Morgan L A 1991 *J. Phys. B: At. Mol. Opt. Phys.* **24** 3685–99
[35] Tennyson J and Noble C J 1984 *Comput. Phys. Commun.* **33** 421
[36] Chakrabarti K, Ghosh R and Choudhury B S 2019 *J. Phys. B: At. Mol. Opt. Phys.* **52** 105205
[37] Munro J J, Harrison S, Fujimoto M M and Tennyson J 2012 *J. Phys.: Conf. Ser.* **388** 012013
[38] Kawate T *et al* 2022 *Nucl. Fusion* **62** 126052